# Top-down lithographic method for inducing strain in carbon nanotubes

Rajay Kumar, Mehmet Aykol,[a] Koungmin Ryu, Chongwu Zhou, and Stephen B. Cronin
*Department of Electrical Engineering, University of Southern California, Los Angeles, California 90089, USA*

(Received 24 November 2008; accepted 5 June 2009; published online 7 July 2009)

We demonstrate a method for inducing strain in carbon nanotubes using standard lithographic techniques. In this work, aligned nanotubes are partially suspended over trenches made by chemical etching. Strain-induced downshifts as high as 31 $cm^{-1}$ are observed in the Raman spectra, roughly corresponding to 1.1% strain. We also observe significant shifts in the resonant transition energy $E_{ii}$ and an irreversible increase in the *D* band Raman intensity. The strains demonstrated using this technique are capable of creating significant bandgaps in metallic nanotubes, greater than $k_BT$ at room temperature, thereby making it possible to convert metallic nanotubes into semiconductors.
 [DOI: 10.1063/1.3159886]

## I. INTRODUCTION

The practical application of carbon nanotubes (CNTs) in electronic circuits has been severely limited by the inhomogeneity of samples, which contain both metallic and semiconducting nanotubes. The main difficulty in utilizing nanotubes as active elements in electronic devices arises from the metallic nanotubes, which short circuit the behavior of the semiconducting nanotubes. Axial straining of CNTs provides a way to create strain-induced bandgaps in the metallic nanotubes, thereby converting them to the more desirable semiconducting state.[1] For practical applications, a top-down method of inducing strain in nanotubes using standard lithographic techniques is much desired. This paper investigates the feasibility of this idea.

Many techniques for generating homogeneous, semiconducting nanotube samples have been investigated by several research groups. These techniques include chemical precipitation of single walled CNTs (SWCNTs) functionalized with octadecylamine in tetrahydrofuran,[2] selective functionalization with diazonium salts,[3] centrifugation after addition of diluted bromine,[4] electrophoresis,[5,6] chromatography,[7] and tuning of catalyst properties.[8,9] In addition, others have tried preferential growth of semiconducting SWCNTs by controlling the conditions of the growth process, chemicals, catalysts, and substrate material.[10] A third approach is to preferentially destroy metallic SWCNTs while leaving the semiconducting ones intact.[11,12] Previous measurements of nanotubes under strain have shown changes in bandgap,[13] electronic transition energies,[14] and phonon energies.[15,16] Several techniques have been investigated for straining CNTs, including atomic force microscope (AFM) manipulation,[17] stretching of elastomeric substrates polydimethylsiloxane,[16,18–20] and the stretching of membranes and epoxy composites containing nanotubes.[21,22]

In this paper, we investigate an alternative technique for straining nanotubes, which involves partially suspending aligned nanotubes across a trench that is progressively made deeper through chemical etching. Upon drying, the large surface tension of the aqueous solution pulls the nanotubes, which are hydrophobic, to the water-air interface. When the water-air interface reaches the bottom of the trench, as the sample is dried, the nanotube is pinned by van der Waals forces to the bottom of the trench in an elongated and, hence, strained state. The large surface forces associated with the drying of liquids are generally considered to be a problem, causing delicate microelectromechanical systems (MEMS) structures to collapse upon drying. This problem is typically avoided by using a critical point dryer, which has become standard practice in MEMS and nanoelectromechanical systems (NEMS) fabrication.[13] Here, we utilize these forces for the purpose of creating strain in nanotubes. The resulting strain is quantified using Raman spectroscopy, which also reveals changes in defect density and electronic transition energies. The geometric configuration of the nanotubes is characterized by atomic force microscopy. Samples created using this method have tens to hundreds of viable nanotubes across each device that can be strained and measured in parallel, making this a scalable technique.

## II. EXPERIMENT

The sample fabrication process consists of several steps, illustrated in Fig. 1(a). Catalyst nanoparticles are deposited on miscut quartz or sapphire substrates by nanosphere lithography. Aligned nanotubes are then grown by chemical vapor deposition from these catalyst islands with $CH_4$ and $C_2H_4$ as the gas feedstock.[10] The aligned nanotubes are then transferred to a silicon wafer with a 600 nm oxide using a pressure-based substrate transfer method, reported previously.[10] A scanning electron microscope (SEM) image of nanotubes grown and deposited using this method is shown in Fig. 1(b). The location of these nanotubes was noted during SEM imaging, enabling their Raman spectra to be subsequently measured. Resonant nanotubes are identified and measured using a Renishaw via Raman microspectrometer. An array of electrodes was deposited by metal evaporation through a shadow mask to produce 50 $\mu$m wide electrodes separated by 3 $\mu$m gaps. The shadow mask is aligned such that the gaps lie perpendicular to the nanotube growth

[a]Electronic mail: memoman.inc@gmail.com.

 

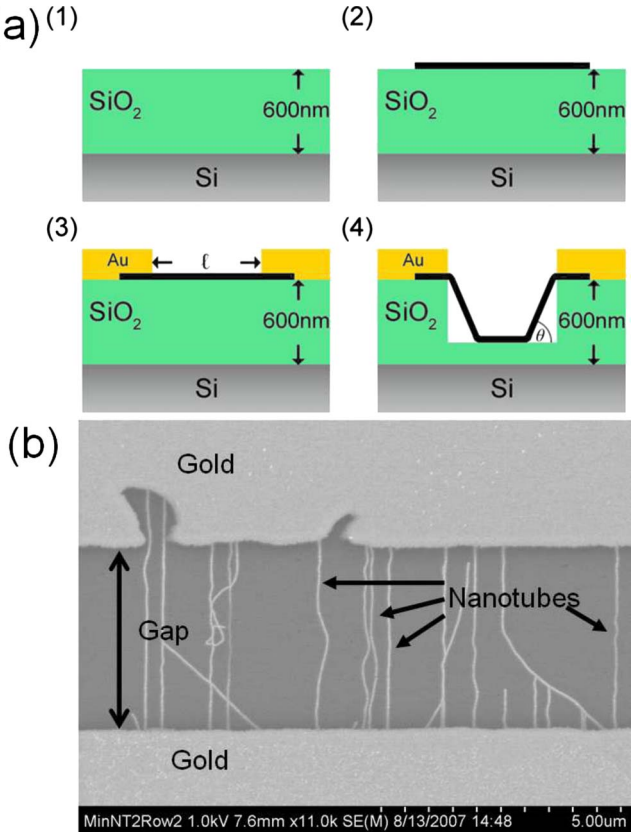


FIG. 1. (Color online) (a) Sample fabrication processing steps. (1) Silicon with 600 nm oxide. (2) Aligned nanotubes are transferred onto substrate. (3) Gold electrodes are deposited using metal evaporation through a shadow mask. (4) An oxide etch is performed by immersion in HF. (b) SEM image of aligned nanotubes between gold electrodes.

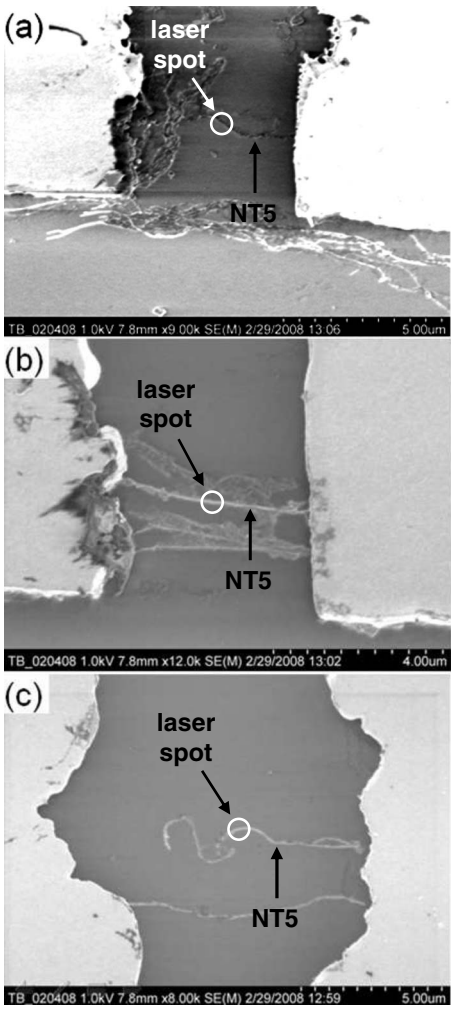


FIG. 2. SEM images of nanotubes after intermediate and final etching. Note the larger width of the trench in (c), as well as the nanotube's relaxed configuration. The white circles indicate the approximate size and position of the laser spot when Raman spectra were taken (Fig. 3).

direction, as shown in Fig. 1(b). The gap is then etched in a bath of hydrofluoric acid (Buffer-HF Improved, Transene Co., Inc., Danvers, MA) and then subsequently rinsed in several baths of water and blow dried with an airgun. The HF acid was empirically found to etch the $SiO_2$ layer of the substrate at a rate of 2.5 nm/s. All steps performed involved standard lithographic techniques only. A Digital Instruments, Dimension 3100 AFM is used to determine the depth of the trench and to characterize the nanotubes' configuration.

## III. RESULTS AND DISCUSSION

Figure 2 shows SEM images of a CNT, NT5, after a sequence of HF etch steps. In our experiment, three etches were performed on five nanotubes that were resonant with a 633 nm wavelength laser. The first etch of 20 s resulted in a 50 nm etch of the underlying $SiO_2$. The second etch of 180 s resulted in an additional 450 nm increase in depth for a total of 500 nm. A third etch, lasting 28 s resulted in an additional 82 nm increase in total depth to 582 nm. From these images, it is apparent that NT5 has broken free from the contact after the final etch and is no longer strained. The approximate size and location of the laser spot when Raman spectra were taken are indicated in these images by the white circles. The *G* band mode ($\sim$1590 $cm^{-1}$) corresponds to the optical phonon in graphene, which splits into two peaks in the nanotube due to its curvature. The vibrational frequency of this mode downshifts with strain, and hence gives a measure of the amount of strain that is applied.[15]

Figure 3 shows the Raman spectra of the nanotube NT5, shown in Fig. 2, taken with a 633 nm laser before and after each HF etch step. The *G* band frequency decreases linearly from 1579 to 1548 $cm^{-1}$, for a total downshift of 31 $cm^{-1}$ due to the strain induced by this process. After the first etch of 50 nm, the *G* band downshifted by 3.6 $cm^{-1}$ from 1579.3 to 1575.7 $cm^{-1}$. The subsequent etch, increasing the trench depth to 500 nm, caused the *G* band to downshift by an additional 27.5–1548.2 $cm^{-1}$. After the final etch, the *G* band reverted to its original prestrain frequency, as shown in Fig. 2(a), indicating a relaxation in strain from erosion of the metal contacts or breakage of the nanotube.

The *D* band intensity increased with these downshifts, as can be seen in Fig. 2. Figure 2(c) shows the ratio of the *D* band to *G* band Raman intensity, plotted as a function of etch depth. The *D* band ($\sim$1325 $cm^{-1}$) involves phonons with finite momentum. Since the photon momentum is much smaller than the phonon momentum, the *D* band is only observed when momentum conservation is broken by disorder. Because of this, the *D* band to *G* band Raman intensity ratio

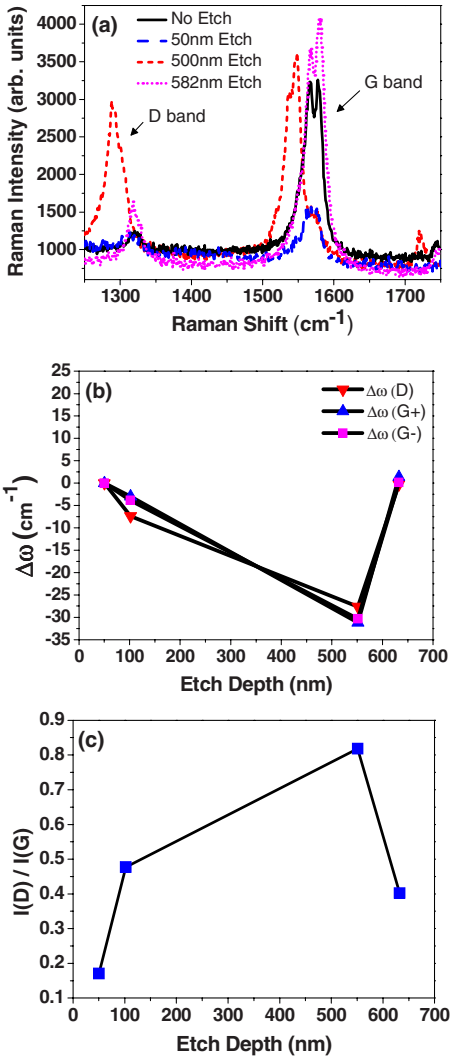


FIG. 3. (Color online) (a) *G* and *D* band Raman spectra of sample NT5 after sequential etches. After the third etch, the high intensity of the *D* band drops and the *G* band upshifts to its pre-etch value. (b) Change in the $G_+$, $G_-$, and *D* band center frequencies plotted as a function of etch depth. (c) Ratio of the *D* band to *G* band Raman intensity plotted as a function etch depth.

can be used to quantify the amount of disorder and defects in nanotubes.[23] After the final etch, the *D* band reverted to a lower intensity, indicating the relaxation of strain-induced defects. This final *D* band intensity, however, was larger than the initial intensity, most likely due to the accumulation of residue on the nanotube surface from precipitate created through the reaction of HF with $SiO_2$.

In addition to etching $SiO_2$, the HF acid is found to produce a residue on the surface of the nanotubes. This can be seen in Figs. 2(a)–2(c). Measurements of the accumulated residue were performed on a prior sample, which underwent a greater number of etches. Figure 4 shows the nanotube height data extracted from AFM cross-sectional analysis. We find the height of the nanotubes to increase rapidly for the first few etches and then saturate to a final thickness of approximately 20 nm. With each etch, the residue accumulates incrementally, showing great increases in height with the initial etches and smaller increases with the final etches. This decline in the rate of accumulation is likely due to particles having fewer available sites to bind to the nanotube surface as more etches are performed.

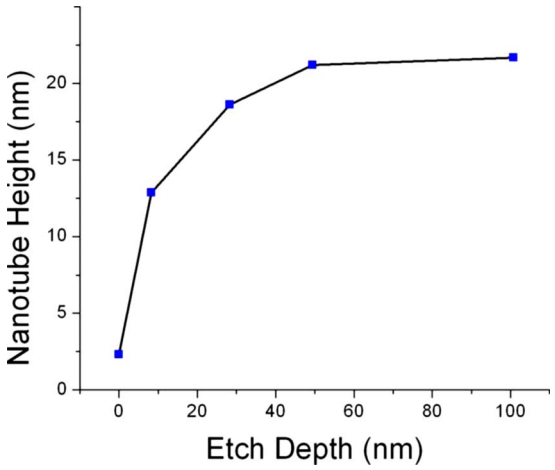


FIG. 4. (Color online) Nanotube height, as determined from AFM cross-sectional analysis, plotted as a function of etch depth.

The nanotube shown in Figs. 2 and 3 exhibited a downshift in the *G* band frequency from 1579 to 1548 $cm^{-1}$, for a total downshift of 31 $cm^{-1}$. Previous measurements have shown the *G* band to downshift at a rate of 28 $cm^{-1}/\%$ axial strain. This implies that roughly 1.1% axial strain was induced in this nanotube by this etched-trench technique. According to tight binding calculations, which have been verified experimentally, strains of this magnitude are capable of inducing bandgaps in metallic nanotubes as large as 0.1 eV.[13,24] The adhesion of the nanotubes to the bottom of the trench results in an elongation of the nanotube from length $\ell$ to $\ell+\Delta\ell$. If the nanotube assumes the configuration shown in Fig. 1(a), part (4), then the elongation is given by

$$\Delta\ell = \frac{2h}{\sin(\theta)} - \frac{2h}{\tan(\theta)}, \tag{1}$$

where $h$ is the etched depth and $\theta$ is the contact angle. For a length $\ell=10$ $\mu$m, an etch depth $h=0.5$ $\mu$m and a contact angle $\theta=20°$, $\Delta\ell/\ell$ is approximately 1.8%. Using this equation, we can calculate the contact angle of the nanotube assuming symmetric contacts for both sides of the nanotube. The nanotube, here, spans an exceptionally wide trench of 11 $\mu$m wide due to irregularly shaped contacts. Given a strain of 1.1% and trench depth of 500 nm, we calculate the contact angle to be 13.8°. This implies that 6.9 $\mu$m of the nanotube is in direct contact with the substrate. For comparison, after the first etch of 50 nm, the contact angle was 15.7°, with only a 10.6 $\mu$m length of nanotube in direct contact with the substrate. Between the first and second etches, almost 35% of the nanotube lost contact with the substrate. While this assumes that there is no initial slack in the nanotubes, these calculations give a rough idea of the geometry of the nanotube after etching and drying.

The isotropic etching of the HF, etches underneath the metal contacts causing many of the nanotubes to break free at one end. Of the five resonant nanotubes measured in this study, only one remained pinned underneath the metal electrodes after the third etch. The other four nanotubes measured in this study became detached from the metallic contacts with increased etching. This failure mechanism is

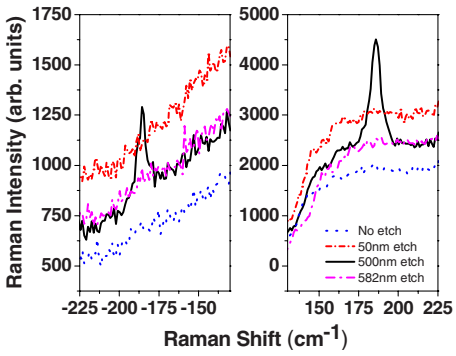


FIG. 5. (Color online) Anti-Stokes (left) and Stokes (right) RBM Raman spectra for sample NT5. Note the prominence of the RBM peak for only the 500 nm etch.

understood on the basis of contact erosion, and can be improved by growing longer nanotubes and/or using shorter trench widths.

The $G'$ band is also observed to downshift significantly with trench depth for the sample shown in Figs. 2 and 3 (NT5). After 50 nm of etching, the $G'$ band frequency downshifts from 2636 to 2625 $cm^{-1}$. When the trench depth reaches 500 nm, the $G'$ band splits into two peaks: a broad peak centered at 2594 $cm^{-1}$ and a narrow peak centered at 2579 $cm^{-1}$. After the final etch where the nanotube relaxes, the peaks cease splitting and upshift to the initial prestrain frequency. The two-peak structure in the $G'$ band has been found in unstrained nanotubes where the $E_{44}^S$ peak is within the resonant window of the laser energy and the $E_{33}^S$ peak is within the resonant window of the scattered photon.[25]

The radial breathing mode (RBM) corresponds to the radial motion of atoms in a nanotube. The RBM frequency is inversely proportional to the diameter of the nanotube.[25] Figure 5 shows the RBM of sample NT5 occurring at 185.5 $cm^{-1}$, with a Stokes/anti-Stokes intensity ratio of 5.3 after 500 nm of etching. This RBM corresponds to a nanotube diameter of 1.3 nm.[26] The appearance of the RBM only after the third etch indicates a strain-induced change in the resonant electronic transition energy $\Delta E_{ii}$ shifting onto resonance with strain. The intensity of the resonant Raman process in nanotubes can be expressed as

$$I(E_l) \propto \left| \frac{1}{(E_l - E_{ii} - i\Gamma_r)(E_l \pm E_{\mathrm{ph}} - E_{ii} - i\Gamma_r)} \right|^2, \qquad (2)$$

where $E_{ii}$ is the resonant transition energy, $E_l$ is the laser energy, $E_{\mathrm{ph}}$ is the phonon energy, and $\Gamma_r$ is the broadening factor for the Raman scattering process.[27] Using Eq. (2), we calculate $\Delta E_{ii}$ to be at least 12.5 meV for a nanotube to shift completely onto (or off of) resonance using $\Gamma_r = 8$ meV, $E_l = E_{ii} = 1.95$ eV, and $E_{\mathrm{ph}} = 23$ meV, which corresponds to the measured value of 185.5 $cm^{-1}$.

Since the ends of the nanotubes lie underneath the metal electrodes, electron transport measurements can be performed on nanotubes spanning the trench after each etch. However, since many nanotubes span each trench, the electrical measurements reflect an ensemble measurement of all the nanotubes, including non-resonant and weakly resonant nanotubes. For the electrodes contacting NT5, we measure the current-voltage ($I$-$V$) characteristics before and after each etch step. After the first etch, the resistance decreased from the pre-etch value of 90–88 kΩ. However, after the second etch, the resistance increased greatly to 4.0 MΩ. This large increase in resistance can be caused by (1) the nanotubes becoming detached from the electrodes, thereby decreasing the total number of nanotubes carrying current between the electrodes, (2) increased scattering by defects induced during the HF etch, and (3) the creation of strain-induced bandgaps in metallic nanotubes. The 2 kΩ decrease observed after the first etch may be due to the removal of residues from the nanotubes or to a decrease in the nanotube/substrate interaction.[28] Since the precise locations of nanotubes are unknown between etches, it is not possible to distinguish the effects of strain, nanotube detachment, and etching of the underlying oxide on the measured electrical behavior. The observed results are most likely a combination of these effects.

## IV. SUMMARY AND CONCLUSION

In this experiment, we demonstrate a method for inducing strain in CNTs using standard lithographic techniques. Upon drying, the large surface tension pulls the suspended nanotubes to the bottom of the trench, thereby inducing strain. The strain is measured by comparing Raman spectra taken before and after etching. We observe strain-induced downshifts in the $G$ band Raman spectra as high as 31 $cm^{-1}$, corresponding to approximately 1.1% strain. This strain is large enough to induce bandgaps in metallic nanotubes larger than $k_BT$ at room temperature. Significant changes in the resonant transition energy, $\Delta E_{ii}$, are corroborated by changes in the resonance condition of the radial breathing mode. The accumulation of residue on the surface of the nanotubes is revealed by atomic force microscopy, reaching 20 nm in thickness. We also observe irreversible increases in the $D$ band Raman intensity, due to chemical damage by the hydrofluoric acid etch and the accumulation of surface residue. Electrical measurements are also performed, revealing an increase in resistivity of the nanotubes, also due to the introduction of defects through the etch process. Since erosion clearly causes the nanotubes to break free from the contacts, future experiments can improve upon this shortcoming by using longer nanotubes and/or shorter trenches. These experiments probe the optical properties of individual resonant nanotubes under strain; however, this technique can be easily scaled to dense arrays of nanotubes.

## ACKNOWLEDGMENTS

This research was supported in part by DOE Award No. DE-FG02-07ER46376.

[1] L. Yang and J. Han, Phys. Rev. Lett. **85**, 154 (2000).
[2] D. Chattopadhyay, I. Galeska, and F. Papadimitrakopoulos, J. Am. Chem. Soc. **125**, 3370 (2003).
[3] M. S. Strano, C. A. Dyke, M. L. Usrey, P. W. Barone, M. J. Allen, H. Shan, C. Kittrell, R. H. Hauge, J. M. Tour, and R. E. Smalley, Science **301**, 1519 (2003).
[4] Z. Chen, X. Du, M.-H. Du, C. D. Rancken, H.-P. Cheng, and A. G. Rinzler, Nano Lett. **3**, 1245 (2003).
[5] R. Krupke, F. Hennrich, H. v. Löhneysen, and M. M. Kappes, Science

**301**(5631), 344 (2003).
[6]W.-J. Kim, M. L. Usrey, and M. S. Strano, Chem. Mater. **19**, 1571 (2007).
[7]D. A. Heller, R. M. Mayrhofer, S. Baik, Y. V. Grinkova, M. L. Usrey, and M. S. Strano, J. Am. Chem. Soc. **126**, 14567 (2004).
[8]Y. Chen, D. Ciuparu, S. Lim, Y. Yang, G. L. Haller, and L. Pfefferle, J. Catal. **226**, 351 (2004).
[9]D. Ciuparu, Y. Chen, S. Lim, G. L. Haller, and L. Pfefferle, J. Phys. Chem. B **108**, 503 (2004).
[10]K. Ryu, A. Badmaev, L. Gomez, F. Ishikawa, B. Lei, and C. Zhou, J. Am. Chem. Soc. **129**, 10104 (2007).
[11]H. Huang, R. Maruyama, K. Noda, H. Kajiura, and K. Kadono, J. Phys. Chem. B **110**, 7316 (2006).
[12]B. Zandian, R. Kumar, J. Theiss, A. W. Bushmaker, and S. B. Cronin, Carbon **47**, 1292 (2009).
[13]E. D. Minot, Y. Yaish, V. Sazonova, J.-Y. Park, M. Brink, and P. L. McEuen, Phys. Rev. Lett. **90**, 156401 (2003).
[14]J. Wu, W. Walukiewicz, W. Shan, E. Bourret-Courchesne, J. W. Ager III, K. M. Yu, E. E. Haller, K. Kissell, S. M. Bachilo, R. B. Weisman, and R. E. Smalley, Phys. Rev. Lett. **93**, 017404 (2004).
[15]S. B. Cronin, A. K. Swan, M. S. Ünlü, B. B. Goldberg, M. S. Dresselhaus, and M. Tinkham, Phys. Rev. Lett. **93**, 167401 (2004).
[16]R. Kumar and S. B. Cronin, Phys. Rev. B **75**, 155421 (2007).
[17]S. B. Cronin, A. K. Swan, M. S. Ünlü, B. B. Goldberg, M. S. Dresselhaus, and M. Tinkham, Phys. Rev. B **72**, 035425 (2005).
[18]H. Maune and M. Bockrath, Appl. Phys. Lett. **89**, 173131 (2006).
[19]J. R. Wood, Q. Zhao, M. D. Frogley, E. R. Meurs, A. D. Prins, T. Peijs, D. J. Dunstan, and H. D. Wagner, Phys. Rev. B **62**, 7571 (2000).
[20]J. R. Wood, Q. Zhao, and H. D. Wagner, Composites, Part A **32**, 391 (2001).
[21]C. Jiang, H. Ko, and V. V. Tsukruk, Adv. Mater. (Weinheim, Ger.) **17**, 2127 (2005).
[22]M. Lucas and R. J. Young, Phys. Rev. B **69**, 085405 (2004).
[23]A. Jorio, M. A. Pimenta, A. G. Souza Filho, R. Saito, G. Dresselhaus, and M. S. Dresselhaus, New J. Phys. **5**, 139 (2003).
[24]L. Yang, M. P. Anantram, J. Han, and J. P. Lu, Phys. Rev. B **60**, 13874 (1999).
[25]M. S. Dresselhaus, G. Dresselhaus, A. Jorio, A. G. Souza Filho, and R. Saito, Carbon **40**, 2043 (2002).
[26]S. M. Bachilo, M. S. Strano, C. Kittrell, R. H. Hauge, R. E. Smalley, and R. B. Weisman, Science **298**, 2361 (2002).
[27]A. Jorio, A. G. Souza Filho, G. Dresselhaus, M. S. Dresselhaus, R. Saito, J. H. Hafner, C. M. Lieber, F. M. Matinaga, M. S. S. Dantas, and M. A. Pimenta, Phys. Rev. B **63**, 245416(R) (2001).
[28]E. Pop, D. Mann, J. Cao, Q. Wang, K. Goodson, and H. Dai, Phys. Rev. Lett. **95**, 155505 (2005).